



## Article

# Assessment of the Performance of TROPOMI NO<sub>2</sub> and SO<sub>2</sub> Data Products in the North China Plain: Comparison, Correction and Application

Chunjiao Wang<sup>1,2</sup>, Ting Wang<sup>1,2,\*</sup>, Pucui Wang<sup>1,2</sup> and Wannan Wang<sup>3</sup>

<sup>1</sup> CNRC & LAGEO, Institute of Atmospheric Physics, Chinese Academy of Sciences, Beijing 100029, China; wangchunjiao@mail.iap.ac.cn (C.W.); pcwang@mail.iap.ac.cn (P.W.)

<sup>2</sup> University of Chinese Academy of Sciences, Beijing 100049, China

<sup>3</sup> Nanyang Institute of Technology, Nanyang 473004, China; wangwn@nyist.edu.cn

\* Correspondence: wangting@mail.iap.ac.cn

**Abstract:** The Tropospheric Monitoring Instrument (TROPOMI) aboard the Sentinel-5 Precursor satellite has been used to detect the atmospheric environment since 2017, and it is of great significance to investigate the accuracy of its products. In this work, we present comparisons between TROPOMI tropospheric NO<sub>2</sub> and total SO<sub>2</sub> products against ground-based MAX-DOAS at a single site (Xianghe) and OMI products over a seriously polluted region (North China Plain, NCP) in China. The results show that both NO<sub>2</sub> and SO<sub>2</sub> data from three datasets exhibit a similar tendency and seasonality. In addition, TROPOMI tropospheric NO<sub>2</sub> columns are generally underestimated compared with collocated MAX-DOAS and OMI data by about 30–60%. In contrast to NO<sub>2</sub>, the monthly average SO<sub>2</sub> retrieved from TROPOMI is larger than MAX-DOAS and OMI, with a mean bias of 2.41 (153.8%) and  $2.17 \times 10^{16}$  molec cm<sup>-2</sup> (120.7%), respectively. All the results demonstrated that the TROPOMI NO<sub>2</sub> as well as the SO<sub>2</sub> algorithms need to be further improved. Thus, to ensure reliable analysis in NCP area, a correction method has been proposed and applied to TROPOMI Level 3 data. The revised datasets agree reasonably well with OMI observations ( $R > 0.95$  for NO<sub>2</sub>, and  $R > 0.85$  for SO<sub>2</sub>) over the NCP region and have smaller mean biases with MAX-DOAS. In the application during COVID-19 pandemic, it showed that the NO<sub>2</sub> column in January–April 2020 decreased by almost 25–45% compared to the same period in 2019 due to the lockdown for COVID-19, and there was an apparent rebound of nearly 15–50% during 2021. In contrast, a marginal change of the corresponding SO<sub>2</sub> is revealed in the NCP region. It signifies that short-term control measures are expected to have more effects on NO<sub>2</sub> reduction than SO<sub>2</sub>; conversely, we need to recognize that although the COVID-19 lockdown measures improved air quality in the short term, the pollution status will rebound to its previous level once industrial and human activities return to normal.

**Keywords:** nitrogen dioxide; sulphur dioxide; TROPOMI; comparison; correction; COVID-19



**Citation:** Wang, C.; Wang, T.; Wang, P.; Wang, W. Assessment of the Performance of TROPOMI NO<sub>2</sub> and SO<sub>2</sub> Data Products in the North China Plain: Comparison, Correction and Application. *Remote Sens.* **2022**, *14*, 214. <https://doi.org/10.3390/rs14010214>

Academic Editors: Syuichi Itahashi, Pawan Gupta, Prabir K. Patra and Simone Lolli

Received: 5 November 2021

Accepted: 30 December 2021

Published: 4 January 2022

**Publisher's Note:** MDPI stays neutral with regard to jurisdictional claims in published maps and institutional affiliations.



**Copyright:** © 2022 by the authors. Licensee MDPI, Basel, Switzerland. This article is an open access article distributed under the terms and conditions of the Creative Commons Attribution (CC BY) license (<https://creativecommons.org/licenses/by/4.0/>).

## 1. Introduction

Nitrogen oxides (NO<sub>x</sub> = NO + NO<sub>2</sub>) and sulphur dioxide (SO<sub>2</sub>) are essential trace gases both in the tropospheric and stratospheric atmosphere, and they are also conventional pollutants that are harmful to human health and ecosystems. China has achieved an incredible growth of economy and urbanization since the 1980s, and meanwhile, environmental deterioration in China has become increasingly severe [1–3]. In the recent decade, the government of China has conducted a series of emission reduction policies and air quality regulations to mitigate air pollution. Since 1995, the Chinese government has paid great attention to harness acid rain and SO<sub>2</sub> pollution and first emphasized the SO<sub>2</sub> emission reduction [4]. After that, the 10th (2001–2005), 11th (2006–2010), 12th (2011–2015) and 13th (2016–2020) five-year plans all set a target of reducing SO<sub>2</sub> and NO<sub>x</sub> emissions and continue insisting upon the goal of energy conservation [5,6]. NO<sub>2</sub> and SO<sub>2</sub> have

been decreasing prominently nationwide since these measures were implemented [7–12]. In addition, an enormous reduction of tropospheric NO<sub>2</sub> levels has been found during the COVID-19 outbreak in 2020 [13–15]. In order to achieve the target of improving air quality, monitoring of these air pollutants and understanding the local pollutants levels are absolutely necessary [16].

Therefore, several satellite-based instruments have been used for air pollution monitoring. Satellite platforms may obtain continuous observations of gas concentrations and provide spatial–temporal distribution over extensive regions. Until now, satellite sensors such as Global Ozone Monitoring Experiment (GOME), SCanning Imaging Absorption spectroMeter for Atmospheric ChartographY (SCIAMACHY), Ozone Monitoring Instrument (OMI), Global Ozone Monitoring Experiment-2 (GOME-2) and TROPospheric Monitoring Instrument (TROPOMI) have demonstrated their ability to measure the NO<sub>2</sub> and SO<sub>2</sub> vertical column density (VCD), and they are utilized in a variety of applications such as investigating the trends of pollutants on a regional or global scale [11,17–19], observing pollutants over a particular area or event (e.g., volcanic SO<sub>2</sub> flux, [20]), evaluating the NO<sub>2</sub> and SO<sub>2</sub> emissions from inverse modelling [3,12,21], and analysing pollutant sources [22].

However, satellite observations also have some basic uncertainties from the instruments themselves and the retrieval algorithm, especially in regions with high pollution levels, and as a result, it is possible to relate space-borne remote sensing records with ground-based (GB) observations to assess and determine the degree of atmospheric pollution. Multi-Axis Differential Optical Absorption Spectroscopy (MAX-DOAS) is one of GB remote sensing technique and has a wide application on a global scale. Jin et al. [23] compared retrievals of tropospheric NO<sub>2</sub> and SO<sub>2</sub> VCDs from a MAX-DOAS equipment with the corresponding OMI observations at a non-urban site over the North China. They revealed the NO<sub>2</sub> columns of two datasets were highly correlated in summer and recommended that further investigation needs to be conducted for SO<sub>2</sub> as its large discrepancies. Theys et al. [24] established a new algorithm for SO<sub>2</sub> inversion based on OMI and validated against MAX-DOAS over the heavily polluted site of Xianghe (China). The comparative results bear a better agreement. Apart from that, Irie et al. [25], Tian et al. [26] and Chan et al. [27] all evaluated the performance of various versions of OMI NO<sub>2</sub> or SO<sub>2</sub> products with GB observations to prove the reliability of OMI records.

Compared to OMI, the TROPOMI has higher spatial and temporal resolution. Several current studies have reported the performance and verification of TROPOMI NO<sub>2</sub> products, e.g., Griffin et al. [28] and Verhoelst et al. [29] compared TROPOMI NO<sub>2</sub> products with multiple GB observations around the world and found a good agreement between the TROPOMI retrievals and in situ observations. Wang et al. [30] presented the comparisons of NO<sub>2</sub> products retrieved by TROPOMI and OMI over China, together with validation against MAX-DOAS over the Xianghe site. It turned out that TROPOMI and OMI showed high correlations in most cases; however, the TROPOMI values were generally underestimated compared with OMI and GB measurements. This means that the improvement of the TROPOMI NO<sub>2</sub> over China is also needed. In addition, Zhao et al. [31], Ialongo et al. [32] and Judd et al. [33] all assessed TROPOMI NO<sub>2</sub> measurements with different methods focused on various regions. In contrast, it is still rare to investigate the performance and accuracy of TROPOMI SO<sub>2</sub> data.

The goals of this study include: (1) evaluation of the TROPOMI tropospheric NO<sub>2</sub> and total SO<sub>2</sub> products against GB observation and OMI records over the polluted region in China; (2) a correction method proposed and applied on TROPOMI Level 3 (L3) daily data; (3) application of the revised TROPOMI dataset during the COVID-19 period. The data and methodology are presented in Sections 2 and 3, respectively. In Section 4, the TROPOMI data are evaluated with correlative OMI and MAX-DOAS measurements and revised by the correction methodology. Then, the corrected NO<sub>2</sub> and SO<sub>2</sub> results are used to investigate the varieties of NO<sub>2</sub> and SO<sub>2</sub> in times of COVID-19. The last two sections describe the discussion and conclusions, respectively.

## 2. Data Description

### 2.1. TROPOMI NO<sub>2</sub> and SO<sub>2</sub> Product

TROPOMI is a hyperspectral imaging spectrometer mounted on the Sentinel-5 Precursor (S5P) satellite, which was launched on 13 October 2017. The S5P spacecraft has a sun-synchronous low earth orbit with local transit time of nearly 13:30. TROPOMI enables an almost daily global scanning resulting from a swath width of 2600 km. The TROPOMI consists of eight bands covering ultraviolet (UV), visible (VIS), near-infrared and short-wave infrared portions of the radiation energy spectrum [34]. In this study, TROPOMI products are used offline (OFFL) version Level 2 (L2) NO<sub>2</sub> (tropospheric NO<sub>2</sub> VCDs) and SO<sub>2</sub> (SO<sub>2</sub> total VCDs) orbit data [35]. The spatial resolution of the TROPOMI NO<sub>2</sub> and SO<sub>2</sub> observations was  $3.5 \times 7 \text{ km}^2$  for the footprint at nadir before 6 August 2019 and refined to  $3.5 \times 5.5 \text{ km}^2$  afterwards. The TROPOMI NO<sub>2</sub> inversion algorithm was developed by the Royal Netherlands Meteorological Institute (KNMI) and built on the heritage of NO<sub>2</sub> DOMINO (Dutch OMI NO<sub>2</sub>) algorithm and QA4ECV community approach with significant improvements [33]. The full technical details could be seen on the TROPOMI science website [36]. For TROPOMI SO<sub>2</sub> product, the algorithm was completed by the Royal Belgian Institute for Space Aeronomy (BIRA-IASB) on the basis of Differential Optical Absorption Spectroscopy (DOAS) technique [37].

The TROPOMI dataset contains a quality assurance value (qa\_value) to indicate the status and quality of the retrieval results, enabling users to conveniently select data for their own purposes. To focus on high quality measurements, the NO<sub>2</sub> and SO<sub>2</sub> records in this work were filtered out with the qa\_value less than 0.75, to exclude part of the pixels covered by snow/ice and cloud (cloud radiance fraction > 0.5) as well as questionable records. Apart from that, only solar zenith angle (SZA) below 75° and 70° for NO<sub>2</sub> and SO<sub>2</sub> pixels, respectively, are considered.

### 2.2. OMI NO<sub>2</sub> and SO<sub>2</sub> Product

OMI, a push room UV–VIS spectrometer, was launched aboard the NASA's EOS-Aura spacecraft on 15 July 2004. The Aura satellite possesses a near-polar, sun-synchronous orbit, and crosses the equator at 13:45 local time. The spatial resolution of OMI is about  $13 \times 24 \text{ km}^2$  at nadir. OMI has been operating for nearly 17 years and still continues to offer precious data for atmospheric research and applications. The data quality and uncertainty of OMI product have been confirmed in the current research. For comparison against TROPOMI retrievals, the OMI NO<sub>2</sub> (OMNO2, Version 003) and SO<sub>2</sub> (OMSO2, Version 003) L2 orbit datasets retrieved by the NASA team [38] are taken into account. OMI products use the normalized spectrum in the VIS ranges (402–465 nm) to obtain the NO<sub>2</sub> slant column densities (SCDs) and then combined with stratospheric and tropospheric air mass factors (AMF) to retrieve VCDs. A detailed description of the OMNO2 product is provided in the README guidance document [39]. In OMSO2 product version 1.2 or later, all SO<sub>2</sub> data records are generated with a retrieval algorithm based on principal component analysis (PCA) algorithm applying a fitting window covering 310.5 to 340 nm [40]. SO<sub>2</sub> column amount we used in this study is an estimate of SO<sub>2</sub> VCD produced with SO<sub>2</sub> Jacobians from a more extensive lookup table and monthly a priori profiles based on model simulations. The SO<sub>2</sub> inversion algorithm is presented in detail by Li et al. [41].

The screening criteria to OMI NO<sub>2</sub> and SO<sub>2</sub> are applied following the recommendations by the user guide, and to minimize comparison error with TROPOMI. Regarding OMI NO<sub>2</sub> filtering, we selected the pixels with the SZA < 75° and effective cloud fraction (CF) < 0.3. For OMI SO<sub>2</sub> filtering, only clear sky scenes, defined as CF less than 0.5, and satellite SZA less than 70° were collected. Additionally, the pixels affected with row anomalies have also been removed before statistical analysis.

### 2.3. MAX-DOAS Measurements

Here, we present almost 2 years (from July 2019 to April 2021) of continuous MAX-DOAS NO<sub>2</sub> and SO<sub>2</sub> observations at the suburban station of Xianghe, China (39.8°N, 117.0°E), a

representative site in a highly polluted area over North China Plain (NCP), about 50 km southeast of Beijing (see Figure 1). This MAX-DOAS instrument is designed by BIRA-IASB and operated by the Institute of Atmospheric Physics (IAP), Chinese Academy of Sciences. The MAX-DOAS focused on the zenith-sky DOAS technique and includes three main components: an optical head installed on a sun tracker, a thermo-regulated box consisting of two spectrometers, and two computers for equipment control and data storage [42]. This setup can measure both scattered and direct sunlight. One of the spectrometers works in UV band (300–390 nm) and another operates in VIS wavelength (400–720 nm). During the observation, the azimuth direction of the telescope is kept to the north. A complete measurement sequence contains 9 elevation viewing angles (2, 4, 6, 8, 10, 12, 15, 30 and 90°) and takes approximately 15 min.

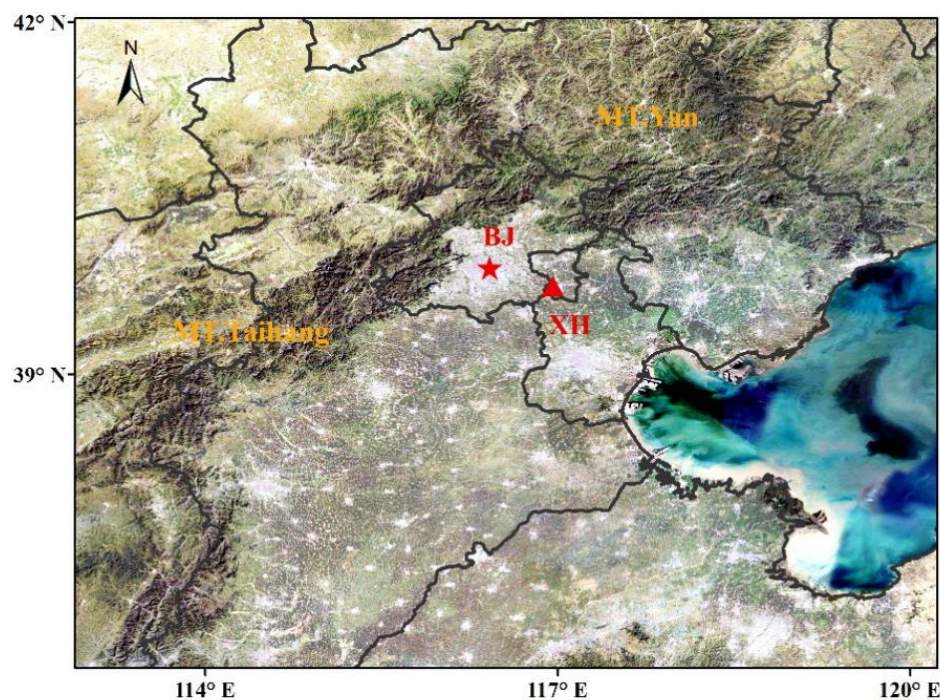


**Figure 1.** Topography overlapped with Beijing (BJ) and Xianghe (XH) Station (red triangle) in North China.

In this study, the QDOAS, a spectral fitting software developed at BIRA-IASB, has been used to analyse the spectra observed from MAX-DOAS. The detailed configuration of retrieval is mentioned in Table 1. The fitting spectral ranges of NO<sub>2</sub> and SO<sub>2</sub> are 425–490 nm and 305–317.5 nm, respectively.

**Table 1.** Settings for NO<sub>2</sub> and SO<sub>2</sub> spectral fitting.

Parameter	Data Source	Trace Gas	
		NO <sub>2</sub>	SO <sub>2</sub>
Fitting interval		425–490 nm	305–317.5 nm
Polynomial degree		5	5
NO <sub>2</sub>	[43], 220 K, 294 K	✓	✓ (only 294 K)
SO <sub>2</sub>	[44], 294 K	×	✓
O <sub>3</sub>	[45], 223 K, 243 K	✓ (only 243 K)	✓
O <sub>4</sub>	[46], 296 K	✓	×
H <sub>2</sub> O	[47], 298 K	✓	×
Ring	Calculated using QDOAS	✓	✓

### 3. Methodology

#### 3.1. Oversampling Method for OMI and TROPOMI L2 Data

To facilitate the comparison of different spaceborne data sources, various data need to be resampled to an equal spatial resolution. We use the inverse distance weighted interpolation (IDW) to resample the L2 satellite records into L3 grid data. Details could be seen in Wang et al. [30]. The distance ( $D_i$ ) from the discrete point ( $x_i, y_i$ ) to the established grid center point ( $x_0, y_0$ ) can be defined as:

$$D_i = \sqrt{(x_0 - x_i)^2 + (y_0 - y_i)^2} \quad (1)$$

and the estimation on grid point  $Z_{(x_0, y_0)}$  can be calculated by:

$$Z_{(x_0, y_0)} = \frac{\sum_{i=1}^n \frac{1}{(D_i)^P} Z_i}{\sum_{i=1}^n \frac{1}{(D_i)^P}} \quad (2)$$

where  $Z_i$  is observed value on each pixel  $i$ ,  $N$  is the total counts of pixels involved in this calculation and  $P$  represents the weight coefficient of distance.

Thus, the daily TROPOMI and OMI L2 observations were binned to  $0.25^\circ \times 0.25^\circ$  grids as the L3 datasets which are used in the subsequent verification, correction and related analysis.

#### 3.2. Corrections Applied to TROPOMI L3 Data

It is assumed that the OMI and TROPOMI have similar observed results on tropospheric  $\text{NO}_2$  and  $\text{SO}_2$  columns, since these two instruments have analogous overpass times (13:45 LST for OMI and 13:30 LST for TROPOMI). Thus, to ensure reliable analysis in NCP area, we improve a mathematical correction method proposed by Huang and Sun [15] and revise the TROPOMI L3 data to reconcile the discrepancies with OMI.

For  $\text{NO}_2$  correction, we obtained the 2-year average difference between OMI and TROPOMI L3 data in 2019 and 2020 as:

$$c_n(i, j) = \text{OMI}_{2\text{year}}(i, j) - \text{TROPOMI}_{2\text{year}}(i, j) \quad (3)$$

where  $c_n(i, j)$  is the mean difference of OMI minus TROPOMI in a grid.  $\text{OMI}_{2\text{year}}$  and  $\text{TROPOMI}_{2\text{year}}$  represent 2-year averages of L3 tropospheric  $\text{NO}_2$  VCDs observed by OMI and TROPOMI, respectively, in 2019 and 2020. The correction item  $c_n(i, j)$  represents the probable sampling and algorithm biases between the different  $\text{NO}_2$  products. The discussion of the stability of correction term is detailed in Section 4.1.

On the basis of Huang's [15] method, we add a deviation coefficient  $a_n$  based on MAX-DOAS  $\text{NO}_2$  results observed in Xianghe, which is defined as:

$$a_n = \frac{\text{TROPOMI}_{2\text{year}} - \text{MAXDOAS}_{2\text{year}}}{[(\text{TROPOMI}_{2\text{year}} - \text{MAXDOAS}_{2\text{year}}) + (\text{OMI}_{2\text{year}} - \text{MAXDOAS}_{2\text{year}})]} \quad (4)$$

Therefore, the corrected TROPOMI  $\text{NO}_2$  in month (or year)  $m_i$  could be expressed as:

$$\text{TROPOMI}_{\text{corr}_{m_i}}(i, j) = \text{TROPOMI}_{m_i}(i, j) + a_n \times c_n(i, j) \quad (5)$$

The correction for TROPOMI  $\text{SO}_2$  is the same as  $\text{NO}_2$  correction. Thus, the correction factor  $c_s(i, j)$  for  $\text{SO}_2$  is similar to  $c_n(i, j)$  which is mentioned in Equation (3), and the deviation coefficient  $a_s$  is also identical to  $a_n$  expressed in Equation (4). The correction method has been applied to correct the TROPOMI L3 dataset over the NCP region and relevant applications have been exhibited in Section 4.

## 4. Results

### 4.1. Evaluation and Correction for TROPOMI Tropospheric NO<sub>2</sub> Data

#### 4.1.1. The Quality of TROPOMI NO<sub>2</sub> Data

The time series of TROPOMI (red dots), OMI (blue dots) tropospheric NO<sub>2</sub> data within a radius of 50 km around Xianghe observatory and the collocated MAX-DOAS measurements are indicated in Figure 2, covering the period July 2019 to April 2021. For MAX-DOAS NO<sub>2</sub> retrievals, we used full-day observed series (light grey dots) as well as the averaged values spanning 12:30 to 14:30 LST based on satellites' overpass time (dark grey dots). The latter is used for quantitative comparison with satellite NO<sub>2</sub> columns. These three observations present the same peaks and mostly abide by the similar day-to-day variability, with maximum values during cold months.

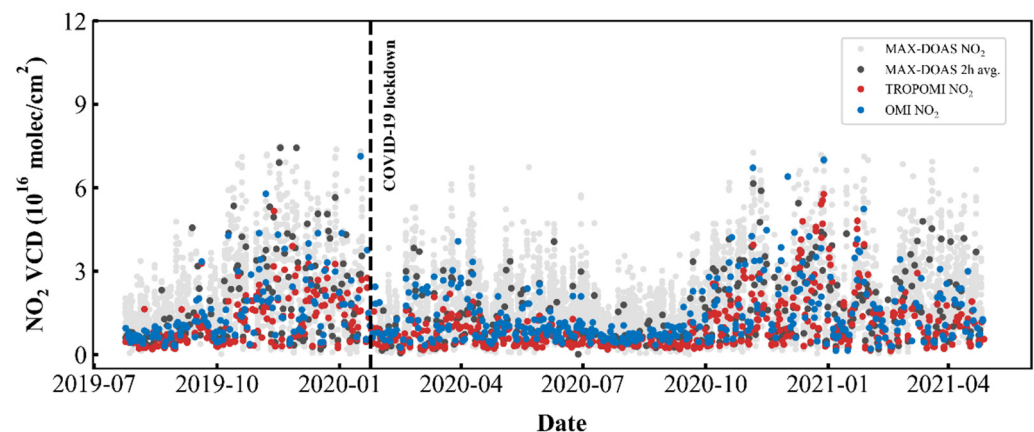


**Figure 2.** Time series of collocated TROPOMI, OMI and GB MAX-DOAS tropospheric NO<sub>2</sub> VCDs during the period from 24 July 2019 to 24 April 2021. Light grey dots denote all the available MAX-DOAS measurements; dark grey dots are the MAX-DOAS retrievals averaged within 2 h (12:30–14:30 LST) before and after satellite overpass time; red and blue dots are TROPOMI and OMI NO<sub>2</sub> data, respectively, within 50 km around Xianghe observatory.

Figure 3 employs the comparison of monthly mean NO<sub>2</sub> values between satellite and GB measurements as well as the corrected TROPOMI L3 datasets. Notably, the monthly mean data only comprised the coincident observation number of correlative days of three datasets. In general, both satellite and GB data show a similar tendency and a strong seasonality, with lowest NO<sub>2</sub> loadings in summer and highest in winter. The seasonality of NO<sub>2</sub> fluctuation is mainly related to the removal mechanisms of the OH radical, which has a similar seasonal cycle [26]. Moreover, satellited-based NO<sub>2</sub> unfolds negative biases relative to MAX-DOAS, and the OMI deviation is smaller and closer to the ground observation, ranging from 20% to 40%. TROPOMI tropospheric NO<sub>2</sub> VCDs are commonly lower than collocated MAX-DOAS by about 30–60%. This finding is consistent with the recent studies of Dimitropoulou et al. [48] and Wang et al. [30]. It is mainly because the representative scales are different between satellite and GB technique [32]. Correlation plots of all related measurements have been shown in Figure 3b. Despite showing negative drifts, the temporal patterns observed from OMI and TROPOMI closely match the GB measurements, since the correlation coefficient (R) values are 0.78 and 0.76 for monthly scales, respectively. The MAX-DOAS and OMI tropospheric NO<sub>2</sub> VCDs are highly correlated with the slope of 0.84, while the slope value (0.60) between MAX-DOAS and TROPOMI indicates that TROPOMI tends to be apparently underestimated.

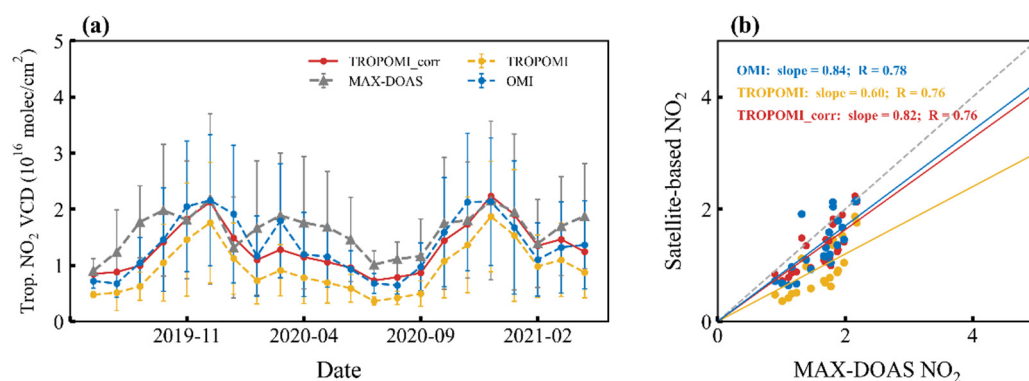


**Figure 3.** (a) Monthly averages of tropospheric NO<sub>2</sub> VCDs based on TROPOMI, OMI, MAX-DOAS and corrected TROPOMI spanning from July 2019 to April 2021. The error bars correspond to the standard deviation. (b) Scatter diagram showing the collocated monthly mean satellited-based and GB NO<sub>2</sub>. The 1:1 line is drawn as a dashed line. Blue, yellow and red lines are OMI, TROPOMI and corrected TROPOMI, respectively (units: 10<sup>16</sup> molec cm<sup>-2</sup>).

Regarding the issue that TROPOMI NO<sub>2</sub> data are underestimated, previous works have investigated the origin of systematic uncertainties in TROPOMI NO<sub>2</sub> retrievals. Boersma et al. [49] presented that primary error sources are mainly attributed to the spectral fitting, the estimation of the stratospheric NO<sub>2</sub> content and uncertainties of ancillary parameters used in AMF calculation (i.e., cloud information, aerosols, surface albedo, and a priori NO<sub>2</sub> profile). For instance, Dimitropoulou et al. [48] discussed the effects of cloud, aerosol, surface albedo and a priori NO<sub>2</sub> profile on inversion results. Specifically, the cloud parameters are used as inputs in a cloud correction scheme applied to NO<sub>2</sub> retrieval that may lead to biases in the tropospheric NO<sub>2</sub> column. Furthermore, TROPOMI NO<sub>2</sub> inversion is prone to be affected by stricter cloud mask (named FRESCO-S) compared with OMI, which presumably removes some heavy pollution cases in the retrievals and induces an underestimation [30]. In addition, aerosols are considered indirectly in the TROPOMI NO<sub>2</sub> algorithm, which means aerosols are processed through the cloud correction scheme. Moreover, they changed the priori vertical profiles measured from MAX-DOAS to recalculate the satellite NO<sub>2</sub> VCDs, leading to a better correlation between the satellite and GB data. Overall, these factors all exert significant impacts on TROPOMI NO<sub>2</sub> inversion.

As a result, to reconcile the discrepancies, the approach shown in Section 3.2 are used to correct TROPOMI NO<sub>2</sub> L3 data. Compared to original results, the corrected TROPOMI results (TROPOMI\_corr for short in Figure 3) are more consistent with MAX-DOS NO<sub>2</sub> column concentrations, with the slope being 0.82 (0.62 in original comparison).

#### 4.1.2. Feasibility Analysis of TROPOMI NO<sub>2</sub> Correction

In order to prove that the correction coefficient  $c_n(i, j)$  is stable within every month and could be used to correct TROPOMI L3 data over the NCP high polluted region, we define the deviation  $\Delta c_{mi}(i, j)$  as:

$$\Delta c_{mi}(i, j) = c_n(i, j) - c_{mi}(i, j) \quad (6)$$

where  $c_{mi}(i, j)$  means the monthly average difference between OMI and TROPOMI of month  $mi$ , and  $\Delta c_{mi}(i, j)$  denotes the deviation value in  $c_n$  and  $c_{mi}$  on each pixel  $(i, j)$ .

Throughout the two years combined, obvious differences prevail in Eastern China between TROPOMI and OMI as shown in panel (a) of Figure 4. Notably, tropospheric NO<sub>2</sub> values derived from the TROPOMI are lower than those from OMI at a nation-wide scale, especially in the NCP (black box highlighted in Figure 4a), where the discrepancies exceed 0.4 ( $\times 10^{16}$  molec cm<sup>-2</sup>). It means that the higher the NO<sub>2</sub> loadings the greater the underestimation. Considering the regionality of MAX-DOAS observations, we produce a corrected TROPOMI L3 dataset over the NCP region. The probability density distribution plot of

$\Delta c_{mi}(i, j)$  is reflected in Figure 4b. The  $\Delta c_{mi}(i, j)$  values denote the deviations derived from the 2-year average difference minus each monthly average difference (OMI-TROPOMI) over the NCP region during the study period, collected with all pixels. Evidently, approximately 80% of  $\Delta c_{mi}(i, j)$  values are lower than regional mean of  $c_n(i, j)$  values (denoted as  $c_{2year}$ , about  $0.34 \times 10^{16}$  molec  $cm^{-2}$ ), indicating the feasibility of the correction term to some extent. Furthermore, the monthly change of regional mean of  $\Delta c_{mi}(i, j)$  is displayed in Figure 4c. The monthly deviation ranges from  $-0.3$  to  $0.2$  ( $\times 10^{16}$  molec  $cm^{-2}$ ), with absolute values less than  $c_{2year}$ . In addition, the positive difference mainly occurs in summer and spring, while the opposite often appears in winter and autumn. These results confirm that the  $c_n(i, j)$  could be used for TROPOMI NO<sub>2</sub> monthly mean data correction most of the time.

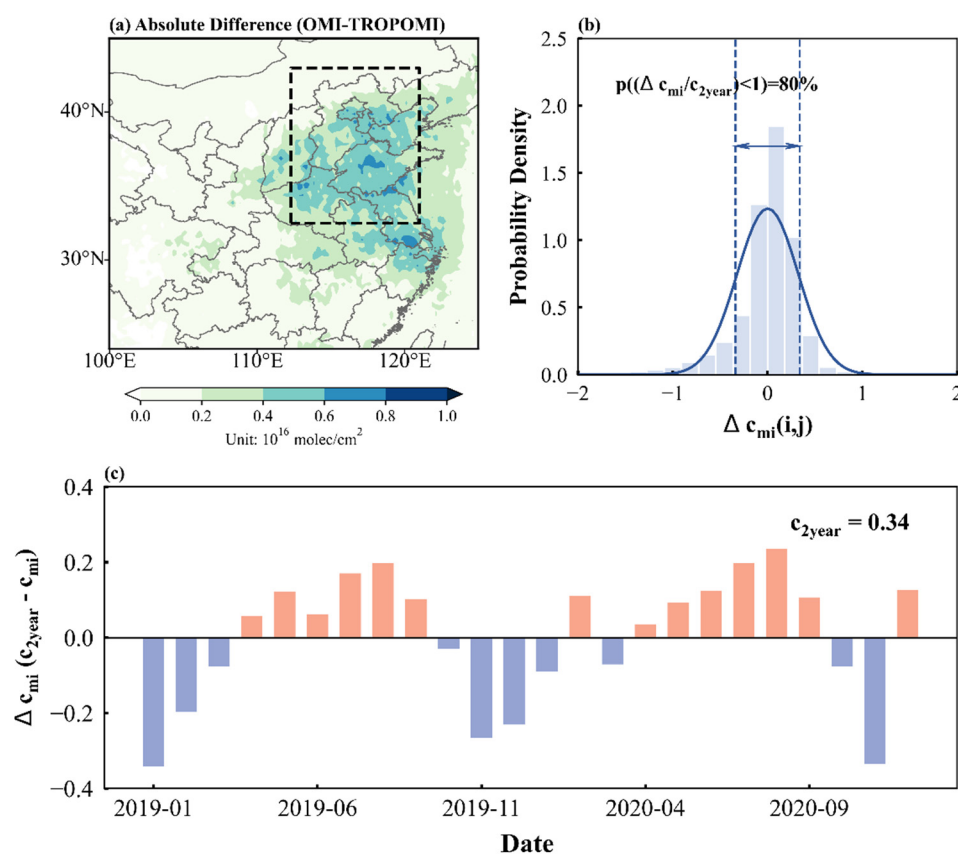


**Figure 4.** (a) The map of the absolute difference between OMI and TROPOMI NO<sub>2</sub> VCDs averaged during 2019 and 2020 (i.e.,  $c_n(i, j)$  in Equation (3)). Black box represents the NCP area. (b) Probability density distribution diagram of the  $\Delta c_{mi}(i, j)$  for all months and all pixels over the NCP region in 2019–2020. (c) Bar-chart plot representing the temporal evolution of the regional mean  $\Delta c_{mi}$  (units:  $10^{16}$  molec  $cm^{-2}$ ).

#### 4.1.3. Correction for TROPOMI NO<sub>2</sub> over the NCP Region

Annual mean geographic distribution of tropospheric NO<sub>2</sub> VCDs over the NCP region observed from OMI, TROPOMI as well as the TROPOMI\_corr are indicated in Figure 5a–c,e–g. The spatial structure from TROPOMI possesses a great resemblance to that from OMI, while the magnitudes in TROPOMI are lower than in OMI. High NO<sub>2</sub> loadings are mainly concentrated around provincial capitals with high emissions. Meanwhile, NO<sub>2</sub> declined significantly in most regions in 2020 compared with 2019, from both OMI and TROPOMI. Application of corrected TROPOMI NO<sub>2</sub> has improved significantly in magnitudes and shows better agreement with OMI observations. The linear regression (Figure 5d,h) yields that the slope of TROPOMI versus OMI increased from 0.59 to 0.86 in

2019 and from 0.63 to 0.93 in 2020. Furthermore, the correlation is much strengthened with the R values raised to 0.99 in these two years.

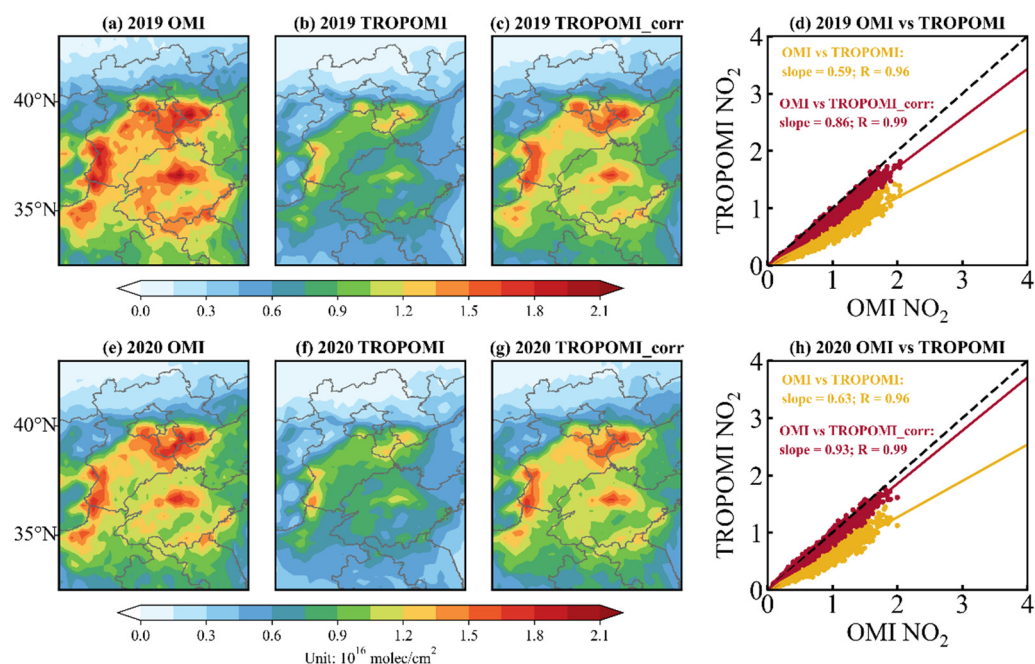


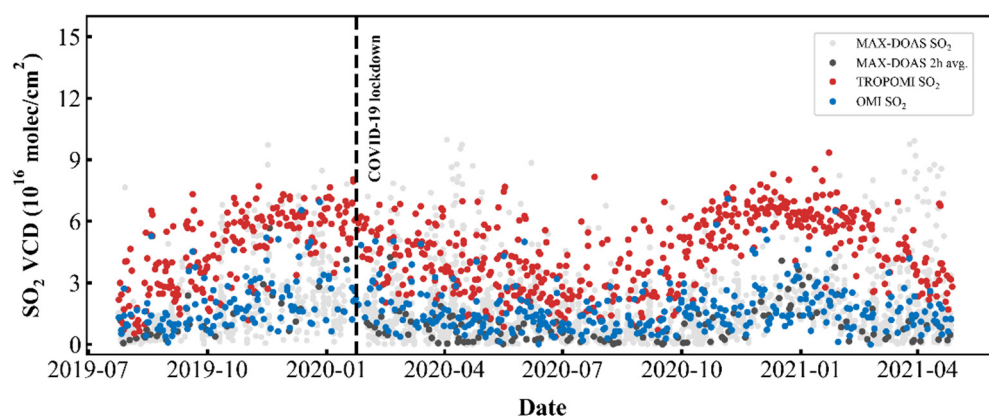
**Figure 5.** Comparisons of annual tropospheric NO<sub>2</sub> VCDs over NCP from OMI and TROPOMI. NO<sub>2</sub> VCDs derived from OMI and TROPOMI in 2019 and 2020 are shown in panels (a,b,e,f), respectively, along with the corrected TROPOMI shown in panels (c,g). Scatter plots of TROPOMI tropospheric NO<sub>2</sub> vs. OMI NO<sub>2</sub> and corrected TROPOMI NO<sub>2</sub> vs. OMI NO<sub>2</sub> in 2019 and 2020 are shown in panels (d,h), respectively.

In brief summary, the TROPOMI, OMI and MAX-DOAS NO<sub>2</sub> VCDs exhibited similar temporal features during the study period at Xianghe site. Compared with GB measurements, the NO<sub>2</sub> VCDs derived from OMI had a regression slope (slope = 0.84) greater than that from TROPOMI (slope = 0.60). Moreover, focusing on the NCP region, the TROPOMI and OMI NO<sub>2</sub> VCDs were strongly correlated ( $R > 0.95$ ) in terms of spatial pattern. However, the magnitudes in the TROPOMI are generally lower than in the OMI by 25% to 35%, particularly over highly contaminated areas in wintertime. Further, the corrected TROPOMI L3 NO<sub>2</sub> datasets have been greatly improved in magnitudes compared with MAX-DOAS and OMI considering either in a single point or over the entire region.

#### 4.2. Evaluation and Correction for TROPOMI Total SO<sub>2</sub> Data

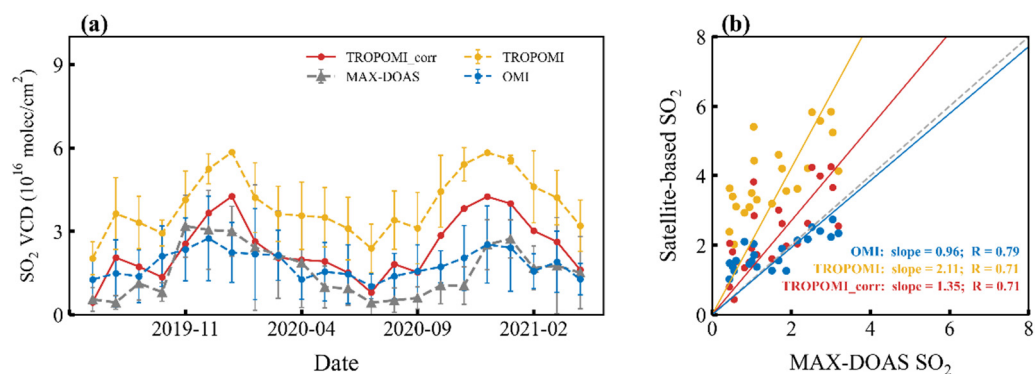
##### 4.2.1. The Quality of TROPOMI SO<sub>2</sub> Data

Figure 6 shows the time series of SO<sub>2</sub> observations at the Xianghe site from July 2019 to April 2021. MAX-DOAS retrieved data are coincidentally averaged in approximately  $\pm 2$  h (12:30 to 14:30 LST) overpass time of TROPOMI and OMI over the target region. The SO<sub>2</sub> VCDs show pronounced seasonal cycle, as evidenced by both remote sensing technique and GB measurement, with a maximum occurring in winter and autumn and a minimum in summer. This marked seasonal fluctuation can be explained by the seasonal feature of emission strengths and lifetimes of the SO<sub>2</sub> as well as the atmospheric transport [23,42]. Moreover, it is obvious that SO<sub>2</sub> VCDs derived from TROPOMI are apparently higher than that from OMI and MAX-DOAS.



**Figure 6.** Same as Figure 2, but for  $\text{SO}_2$ .

To better explore  $\text{SO}_2$  monthly variation and satellite product quality, the monthly  $\text{SO}_2$  VCDs from space-based and GB measurements are performed. As shown in Figure 7, the monthly mean  $\text{SO}_2$  columns from MAX-DOAS are well covariates with the OMI data ( $R = 0.79$ ), and their magnitudes are in great agreement (slope = 0.96), implying well-captured monthly variations. In contrast, differences among TROPOMI-inferred  $\text{SO}_2$  (marked in yellow line) and those of OMI and MAX-DOAS observations feature a slightly lower agreement ( $R = 0.71$  with MAX-DOAS) and an order of magnitude difference (slope = 2.11 with MAX-DOAS) with TROPOMI typically overvalued. Based on the better consistency between the OMI and MAX-DOAS  $\text{SO}_2$  VCDs, a method for TROPOMI  $\text{SO}_2$  correction is developed.



**Figure 7.** (a) Same as Figure 3a, but for  $\text{SO}_2$ . (b) Same as Figure 3b, but for  $\text{SO}_2$ .

In the following, we present the corrected  $\text{SO}_2$  results derived from the correction technique introduced above (detailed in Section 3.2). The corresponding plot is also presented in Figure 7. For comparison of corrected TROPOMI and MAX-DOAS, slope is higher than 1 (slope = 1.35), suggesting that corrected TROPOMI observations still provide higher values than MAX-DOAS in several months, especially in wintertime. However, slope values of corrected  $\text{SO}_2$  VCDs are close to 1 than that of original results (slope = 2.11), also indicating better agreement of corrected TROPOMI  $\text{SO}_2$  in terms of monthly mean values.

#### 4.2.2. Feasibility Analysis of TROPOMI $\text{SO}_2$ Correction

Referring to the previous analysis, a verification for stability of correction coefficient  $c_s(i, j)$  was performed. As shown in Figure 8a, the absolute difference in  $\text{SO}_2$  analysis is defined as TROPOMI minus OMI, which is different with in  $\text{NO}_2$ . The discrepancy is about  $1.5$  to  $3.0 \times 10^{16}$  molec  $\text{cm}^{-2}$  over NCP area, indicating overestimated  $\text{SO}_2$  values that are apparent in the TROPOMI measurements throughout the entire research area. Moreover, the TROPOMI  $\text{SO}_2$  product exhibits severe  $\text{SO}_2$  pollution in most areas of China, which is inconsistent with the fact that  $\text{SO}_2$  emissions have been reduced significantly in China [50].

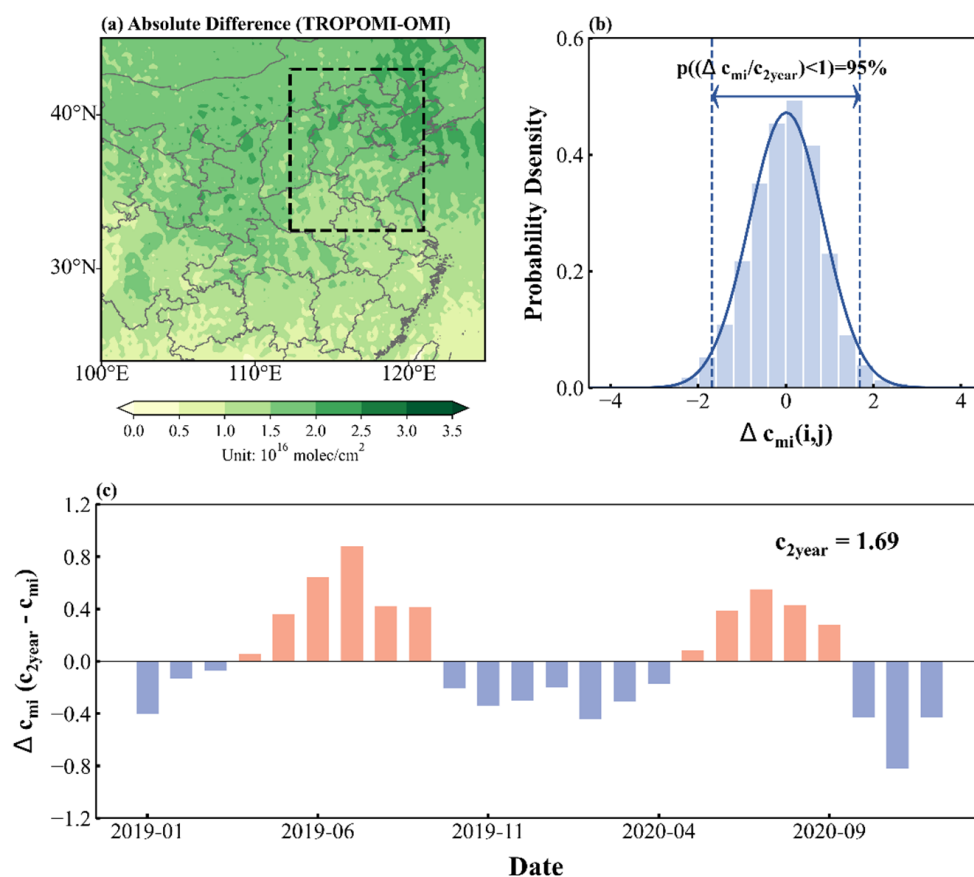


**Figure 8.** (a) The map of the absolute difference between TROPOMI and OMI SO<sub>2</sub> VCDs averaged during 2019 and 2020 (i.e.,  $c_s(i, j)$  in Equation (3)). Black box represents the NCP area. (b) Probability density distribution diagram of the  $\Delta c_{mi}(i, j)$  for all months and all pixels over the NCP region in 2019–2020. (c) Bar-chart plot representing the temporal evolution of the regional mean  $\Delta c_{mi}$  (units:  $10^{16}$  molec  $\text{cm}^{-2}$ ).

The probability density distribution plot of  $\Delta c_{mi}(i, j)$  is also shown in panel (b) of Figure 8. The definition of  $\Delta c_{mi}(i, j)$  for SO<sub>2</sub> is analogous to that of NO<sub>2</sub>. As we can see, approximately 95% of  $\Delta c_{mi}(i, j)$  values are lower than regional mean of  $c_s(i, j)$  value (denoted as  $c_{2\text{year}}$ , about  $1.69 \times 10^{16}$  molec  $\text{cm}^{-2}$ ), which means that the  $c_s(i, j)$  is reasonable to be used in each month correction. Considering the monthly change of regional mean of  $\Delta c_{mi}(i, j)$  in Figure 8c, the monthly deviation values are within  $\pm 0.8$  ( $\times 10^{16}$  molec  $\text{cm}^{-2}$ ), larger than that of NO<sub>2</sub> (within  $\pm 0.3 \times 10^{16}$  molec  $\text{cm}^{-2}$ ). Therefore, the magnitudes of the TROPOMI SO<sub>2</sub> retrievals need further correction and validation.

#### 4.2.3. Correction for TROPOMI SO<sub>2</sub> over the NCP Region

Comparison results of TROPOMI, OMI and TROPOMI\_corr SO<sub>2</sub> results in 2019 and 2020 are plotted in Figure 9. Large SO<sub>2</sub> columns are standing out over the NCP region. The retrievals by TROPOMI and OMI both reveal similar spatial distribution of the SO<sub>2</sub> loadings, while the magnitudes in TROPOMI are much higher than in OMI. In terms of the whole NCP area, the spatial correlations in annual mean SO<sub>2</sub> VCDs between the TROPOMI and OMI remained poor in some regions and the R values in 2019 and 2020 are 0.37 and 0.41, respectively. When the correction method is applied, TROPOMI SO<sub>2</sub> datasets are greatly improved, not only in regional distribution but also in magnitudes, with R values increased to above 0.85. As we know, the retrieval accuracy of SO<sub>2</sub> columns from TROPOMI is also limited by several factors, such as uncertainties of SCDs inversion and the AMF calculations. For instance, the SO<sub>2</sub> is not easy to be extracted as its low content in the atmosphere; and the absorption of SO<sub>2</sub> is weaker than that of O<sub>3</sub> in the equal

wavelengths, which could be disturbed in the process of spectral fitting [50]. For another example, according to the research of Theys et al. [24], they considered potential factors causing errors in SO<sub>2</sub> retrievals, including the priori profile. They found that the OMI columns, which are corrected by the MAX-DOAS profile shape, agree very well with GB records. Moreover, Xia et al. [50] used a priori profile from GEOS-Chem schema instead of from TM5 simulations in TROPOMI SO<sub>2</sub> inversion, the relative bias between TROPOMI SO<sub>2</sub> results and MAX-DOAS observations descended from 17.9–28.4% to 11.2–12.4%. This illustrates the importance of a priori profiles on the SO<sub>2</sub> inversion.

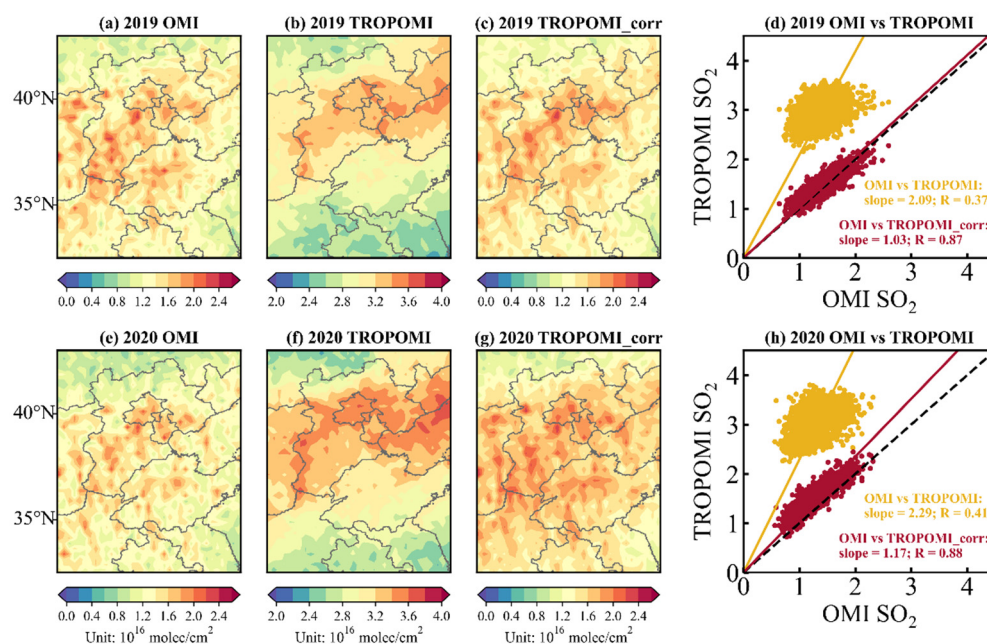


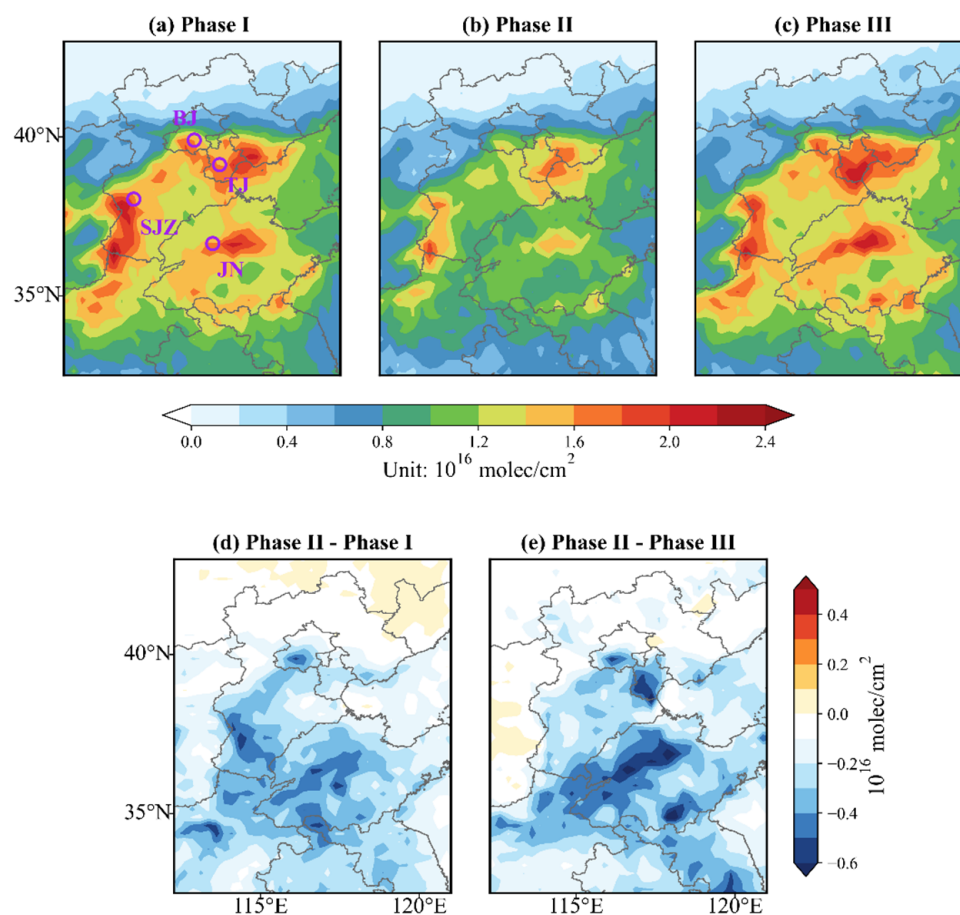
**Figure 9.** Comparisons of annual SO<sub>2</sub> VCDs over NCP from OMI and TROPOMI. SO<sub>2</sub> VCDs derived from OMI and TROPOMI in 2019 and 2020 are shown in panels (a,b,e,f), respectively, along with the corrected TROPOMI shown in panels (c,g). Scatter plots of TROPOMI SO<sub>2</sub> vs. OMI SO<sub>2</sub> and corrected TROPOMI SO<sub>2</sub> vs. OMI SO<sub>2</sub> in 2019 and 2020 are shown in panels (d,h), respectively.

In short, the TROPOMI inversions could capture the SO<sub>2</sub> temporal manners in general but tended to overstate the magnitudes over Xianghe observatory. For comparison of TROPOMI and OMI SO<sub>2</sub> over the NCP region, the apparent overestimation could also be found in TROPOMI, and weak spatial correlations ( $R < 0.45$ ) were demonstrated. The corrected TROPOMI SO<sub>2</sub> L3 data are closer to OMI in magnitude and the correlation over the entire region has also increased. Inter-comparisons of the TROPOMI and MAX-DOAS SO<sub>2</sub> columns indicate that the inversion algorithm of TROPOMI SO<sub>2</sub> needs further improvement, especially in the heavily polluted areas over China.

#### 4.3. Analysis of NO<sub>2</sub> and SO<sub>2</sub> over NCP during COVID-19 Period

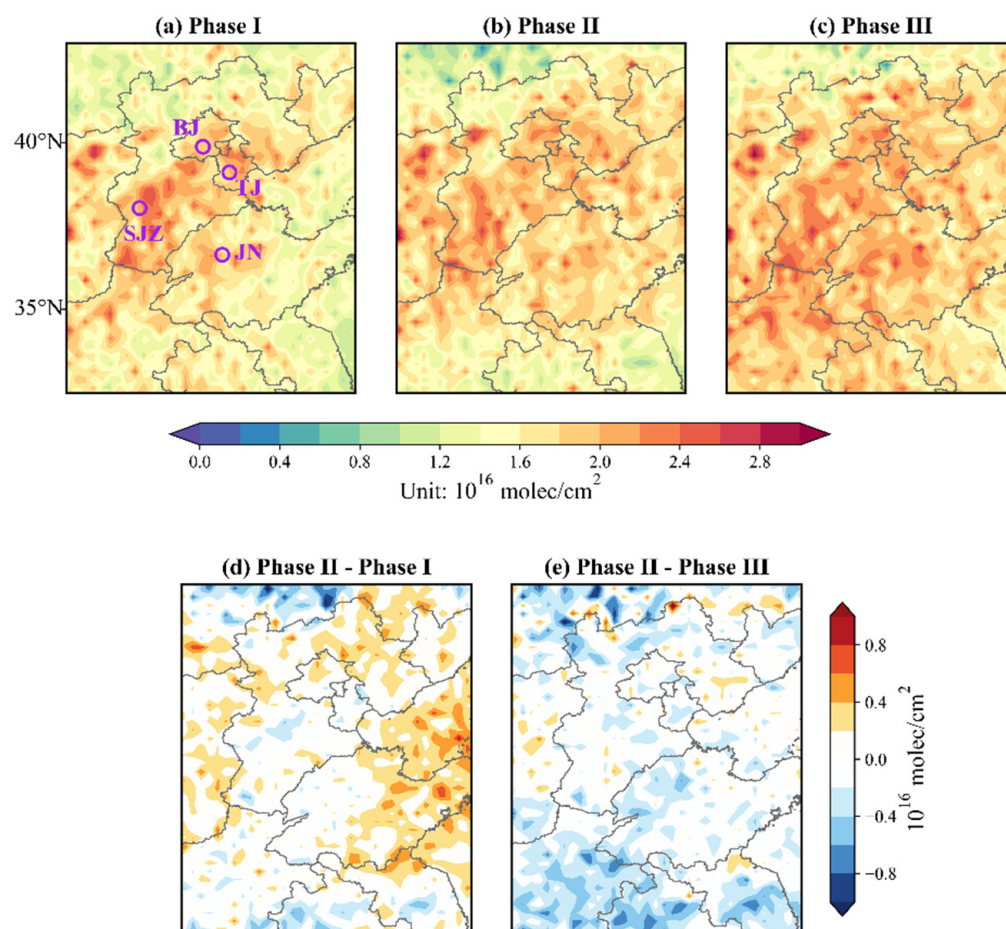
The global lockdown caused by the coronavirus disease (COVID-19) pandemic in 2020 reduced social and economic activities in China. The Chinese government implemented a strict lockdown measure in Wuhan on January 23. By then, a lockdown was enforced in Wuhan and extended to nationwide until 8 April 2020. Based on the corrected NO<sub>2</sub> and SO<sub>2</sub> TROPOMI L3 datasets, we investigated the responses of the NO<sub>2</sub> and SO<sub>2</sub> levels resulting from the spread of COVID-19 over the NCP region. Average NO<sub>2</sub> columns during January to April in 2019, 2020 (lockdown period) and 2021 are referred to as Phase I, Phase II and Phase III, respectively. Note that the lunar new year holidays in 2019 range from 4 February to 10 February, in 2020 from 24 January to 31 January, and in 2021 from 11 February to 17 February, which are all included in our research period. Therefore, the impact of “holiday effect” is not considered separately.

Figure 10 presents the spatial pattern of time-averaged NO<sub>2</sub> columns over NCP into three phases. Regarding NO<sub>2</sub>, high contents are shown in the provincial capitals and their surrounding areas, and broad-scale reductions by 25% to 45% are prevalent in NCP during Phase II. The reduction pattern shown in Figure 10d implies a substantial reduction in economic activities and human migration during this period. During Phase III, when the epidemic prevention and control gradually alleviated, the NO<sub>2</sub> concentrations exhibit a rapid and sharp increase, with highest amplification in the areas surrounding Tianjin (TJ) and Jinan (JN) by about up to 60%. Overall, the lockdown measure during COVID-19 had a significant effect on NO<sub>2</sub> reductions over the entire NCP area. After that, a prominent rebound trend was noted in the same period in 2021.



**Figure 10.** (a–c) Tropospheric NO<sub>2</sub> VCDs from corrected TROPOMI in North China for Phase I (before COVID-19), Phase II (COVID-19 lockdown) and Phase III (after COVID-19 lockdown) periods. (d) The differences between Phase II and Phase I. (e) The differences between Phase II and Phase III. Circle markers indicate major capital cities over this region. From top to bottom are Beijing (BJ), Tianjin (TJ), Shijiazhuang (SJZ) and Jinan (JN) (units:  $10^{16}$  molec  $\text{cm}^{-2}$ ).

According to the NO<sub>2</sub> decrease, a SO<sub>2</sub> reduction is also expected during COVID-19. However, unlike previous conclusions, SO<sub>2</sub> columns did not change obviously during the blockade period. As shown in Figure 11, compared to Phase I, the differences in most areas are about  $-0.4$  to  $0.4 \times 10^{16}$  molec  $\text{cm}^{-2}$  (approximately  $-0.15$  to  $0.15$  DU,  $1 \text{ DU} = 2.687 \times 10^{16}$  molec  $\text{cm}^{-2}$ ), suggesting that SO<sub>2</sub> concentration remains fairly stable throughout Phase I and Phase II. Taking into account Phase III, the SO<sub>2</sub> columns still keep stable compared with Phase II, with slightly increased only in some places about 10–20%. It manifests that control measures during COVID-19 have negligible impact on atmospheric SO<sub>2</sub>.



**Figure 11.** (a–c) SO<sub>2</sub> VCDs from corrected TROPOMI in North China for Phase I (before COVID-19), Phase II (COVID-19 lockdown) and Phase III (after COVID-19 lockdown) periods. (d) The differences between Phase II and Phase I. (e) The differences between Phase II and Phase III. Circle markers indicate major capital cities over this region. From top to bottom are Beijing (BJ), Tianjin (TJ), Shijiazhuang (SJZ) and Jinan (JN) (units:  $10^{16}$  molec  $\text{cm}^{-2}$ ).

In general, high NO<sub>2</sub> accumulation was similar to SO<sub>2</sub>, which may appear over the similar hot spots in North China. For quantitative comparison, four major capital cities over this target region have been given and discussed in Figure 12. The tropospheric NO<sub>2</sub> columns in all spots experienced a dramatic drop during Phase II and then recovered progressively. Specifically, the NO<sub>2</sub> VCDs decreased by 0.28, 0.22, 0.39 and 0.38  $\times 10^{16}$  molec  $\text{cm}^{-2}$  in Beijing (BJ), TJ, Shijiazhuang (SJZ) and JN areas, respectively, between Phase I and Phase II, reflecting overall lower emissions during this period. Then, significant growth appeared in phase III, indicating that a recovery to previous years after the epidemic remission is expected. As for SO<sub>2</sub>, the columns in the lockdown period (Phase II) have changed little versus during the same period of Phase I. Subsequently, in Phase III, SO<sub>2</sub> levels in the four regions increased slightly, with the highest increase in JN by about 15.8%.

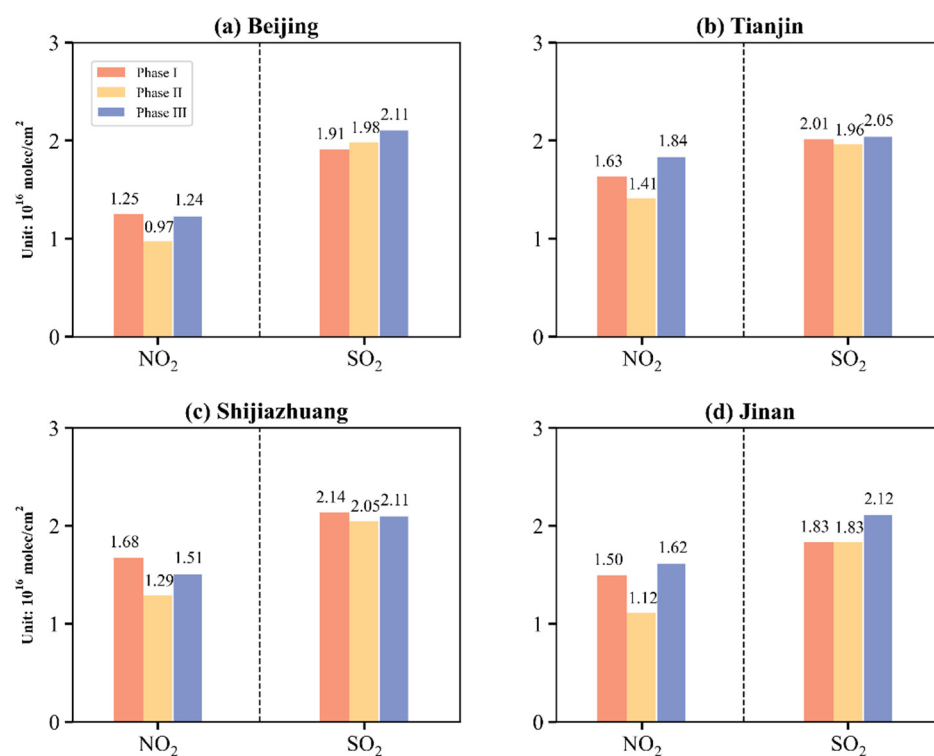


**Figure 12.** Bar graphs of NO<sub>2</sub> and SO<sub>2</sub> changes in three phases of four major capital cities: (a) Beijing, (b) Tianjin, (c) Shijiazhuang and (d) Jinan (units: 10<sup>16</sup> molec cm<sup>-2</sup>).

In sum, the NO<sub>2</sub> levels during Phase II were overall significantly lower than in Phase I, and the NO<sub>2</sub> levels may quickly rebound when public activities in China are resumed. However, SO<sub>2</sub> changes were less pronounced during COVID-19. Thus, the restrictive measures that China had implemented to respond to COVID-19 had a more obvious influence on NO<sub>2</sub>. In addition, although the air quality has been improved in the short term due to the lockdown measures during COVID-19, the pollution status will rebound to its previous level at once the industrial and human activities return to normal levels.

## 5. Discussion

The results from the present comparison analysis could improve our understanding of the quality of TROPOMI products in China, especially the validation and investigation of SO<sub>2</sub>, which is still scarce in current research.

Throughout the analysis above, we found that both the diurnal and monthly NO<sub>2</sub> and SO<sub>2</sub> variability are revealed well by the TROPOMI, in accordance with OMI and MAX-DOAS measurements in Xianghe site, displaying an evident seasonal characteristic with highest in winter and lowest in summer. However, some uncertainties also exist over highly polluted areas, especially for SO<sub>2</sub> data, which cannot well reflect the current pollution status in China. Therefore, combining with other satellite and ground-based dataset, we provided an attempt to correct TROPOMI dataset, hoping to improve its accuracy and make it more consistent with the real pollution situation in China. In other parts of China, this method could also be applied with reliable satellite and ground-based data. In addition, we need to realize that the error source analysis of TROPOMI data products and the improvement of algorithm process over China are still necessary.

When using the modified dataset to study the environmental pollution situation before and after COVID-19 over the NCP area, we found that NO<sub>2</sub> experienced a process of rising first and then reducing. In fact, several epidemic-related studies have confirmed the fact that NO<sub>2</sub> levels decreased significantly during COVID-19 in 2020, as shown in Bauwens et al. [13], Fan et al. [14], Huang and Sun [15] and Filonchyk et al. [51]. In this study, a comparison of the same period in 2021 also confirms that NO<sub>2</sub> has returned to pre-

epidemic (in 2019) levels without the strict lockdown policy. In contrast, SO<sub>2</sub> concentrations did not fluctuate significantly before and after COVID-19. Although, in the study of Fan et al. [14] and Filonchik et al. [51], slight declines in SO<sub>2</sub> concentrations also appeared in certain areas and cities during COVID-19 (in 2020). However, compared with the sharp decline of NO<sub>2</sub>, the change of SO<sub>2</sub> seems not obvious. Considering the reasons for this phenomenon, we also made some reasonable guesses. As mentioned in Filonchik et al. [51], they showed that SO<sub>2</sub> levels decreased slightly in February 2020, compared with February 2019, and coal consumption in power plants and factories recovered to previous levels by the end of March, restoring SO<sub>2</sub> levels to normal. In addition, at the same stage in 2021, SO<sub>2</sub> still remains stable, and similar finding is also mentioned in the study of Wang et al. [52]. They found that SO<sub>2</sub> changes were not statistically significant over the NCP region during the Asian-Pacific Economic Cooperation (APEC) in 2014, showing that the SO<sub>2</sub> reduction was more related to natural or random variability rather than external forcing. Similarly, the specific factors causing such changes in NO<sub>2</sub> and SO<sub>2</sub> during COVID-19 still need further experiments and discussions.

## 6. Conclusions

In this study, column NO<sub>2</sub> and SO<sub>2</sub> data derived from TROPOMI/S5P were evaluated against ground-based MAX-DOAS at a single site (Xianghe) from 2019 to 2021. Comparison between TROPOMI retrievals and OMI products over a highly polluted region (NCP) are also conducted. It was found that satellited-based NO<sub>2</sub> data are both negatively biased relative to MAX-DOAS, and the OMI deviation is smaller and closer to the ground observation, ranging from 20% to 40%. Meanwhile, TROPOMI tropospheric NO<sub>2</sub> VCDs are slightly lower than collocated MAX-DOAS observations by about 30–60%. When it comes to SO<sub>2</sub>, the monthly average SO<sub>2</sub> column retrieved from TROPOMI is larger than MAX-DOAS and OMI, with a mean bias of 2.41 (153.8%) and  $2.17 \times 10^{16}$  molec cm<sup>-2</sup> (120.7%) at Xianghe site, respectively. MAX-DOAS comparisons to OMI are more correlated than TROPOMI during the investigated time ( $R = 0.79$  vs.  $0.71$ ). SO<sub>2</sub> VCDs derived from TROPOMI seem overestimated and the algorithm needs to be further improved in the future.

After the correction, TROPOMI NO<sub>2</sub> and SO<sub>2</sub> displayed markedly better consistencies with OMI in both magnitudes and distribution over the NCP area. The  $R$  values for regional mean concentrations increased greater than 0.95 and 0.85 for NO<sub>2</sub> and SO<sub>2</sub>, respectively.

Finally, we used the corrected TROPOMI NO<sub>2</sub> and SO<sub>2</sub> dataset to investigate the environmental pollution status during COVID-19 period over the NCP region. Evident decreases in NO<sub>2</sub> columns were shown in the lockdown period (Phase II) compared to the same period in 2019 (Phase I), reduced by almost 25–45%, while SO<sub>2</sub> concentration remains fairly stable throughout Phase I and Phase II. Then, NO<sub>2</sub> and SO<sub>2</sub> levels observed from TROPOMI returned to normal in Phase III. This implies that the lockdown measure during COVID-19 had a certain inhibitory effect on environmental pollution and are expected to be more effective on NO<sub>2</sub> reduction than SO<sub>2</sub>. Although the air quality was improved in the short term due to the lockdown measures during COVID-19, the pollution levels may rebound to their previous level once industrial and human activities return to original levels.

Overall, these works will help the assessment and algorithm improvement work for future TROPOMI NO<sub>2</sub> and SO<sub>2</sub> products, and further studies are also needed to investigate the causes of such errors of the NO<sub>2</sub> and SO<sub>2</sub> inversion over China.

**Author Contributions:** C.W. and W.W. conceived and designed the experiments; C.W. prepared and processed the data; T.W. and P.W. maintained the ground-based instrument; C.W. finalized the original draft; T.W., P.W. and W.W. provided useful comments which improved the paper. All authors have read and agreed to the published version of the manuscript.

**Funding:** The work is supported by the National Key R&D Program of China (No. 2021YFB3901000), the National Natural Science Foundation of China (No. 41575034), and the National Key R&D Program of China (No. 2021YFE0118000).

**Data Availability Statement:** The TROPOMI NO<sub>2</sub> and SO<sub>2</sub> data are publicly available at ESA Copernicus Open Access Hub: <https://s5phub.copernicus.eu/>, accessed on 4 November 2021. The OMI NO<sub>2</sub> and SO<sub>2</sub> data are publicly available at: <https://disc.gsfc.nasa.gov/>, accessed on 4 November 2021. The ground-based data presented in this study are available on request from the corresponding author.

**Acknowledgments:** We acknowledge TROPOMI and OMI science teams for making TROPOMI and OMI Level 2 data publicly available. We are thankful to Lushuai Zhou and Sihong Zhu for the technical support. We also thank the reviewers and editors for their invaluable comments, which have improved the manuscript.

**Conflicts of Interest:** The authors declare no conflict of interest.

## References

- Schneider, P.; Lahoz, W.A.; van der A, R. Recent satellite-based trends of tropospheric nitrogen dioxide over large urban agglomerations worldwide. *Atmos. Chem. Phys.* **2015**, *15*, 1205–1220. [CrossRef]
- Krotkov, N.A.; McLinden, C.A.; Li, C.; Lamsal, L.N.; Streets, D.G. Aura OMI observations of regional SO<sub>2</sub> and NO<sub>2</sub> pollution changes from 2005 to 2015. *Atmos. Chem. Phys.* **2016**, *16*, 4605–4629. [CrossRef]
- Meng, K.; Xu, X.; Cheng, X.; Xu, X.; Qu, X.; Zhu, W.; Ma, C.; Yang, Y.; Zhao, Y. Spatio-temporal variations in SO<sub>2</sub> and NO<sub>2</sub> emissions caused by heating over the Beijing-Tianjin-Hebei Region constrained by an adaptive nudging method with OMI data. *Sci. Total Environ.* **2018**, *642*, 543–552. [CrossRef] [PubMed]
- Zhang, X.; van Geffen, J.; Liao, H.; Zhang, P.; Lou, S. Spatiotemporal variations of tropospheric SO<sub>2</sub> over China by SCIAMACHY observations during 2004–2009. *Atmos. Environ.* **2012**, *60*, 238–246. [CrossRef]
- Zhao, P.; Tuygun, G.T.; Li, B.; Liu, J.; Yuan, L.; Luo, Y.; Xiao, H.; Zhou, Y. The effect of environmental regulations on air quality: A long-term trend analysis of SO<sub>2</sub> and NO<sub>2</sub> in the largest urban agglomeration in southwest China. *Atmos. Pollut. Res.* **2019**, *10*, 2030–2039. [CrossRef]
- Wang, C.; Wang, T.; Wang, P. The Spatial–Temporal Variation of Tropospheric NO<sub>2</sub> over China during 2005 to 2018. *Atmosphere* **2019**, *10*, 444. [CrossRef]
- Lu, Z.; Streets, D.G.; Zhang, Q.; Wang, S.; Carmichael, G.R.; Cheng, Y.F.; Wei, C.; Chin, M.; Diehl, T.; Tan, Q. Sulfur dioxide emissions in China and sulfur trends in East Asia since 2000. *Atmos. Chem. Phys.* **2010**, *10*, 6311–6331. [CrossRef]
- Li, C.; Zhang, Q.; Krotkov, N.A.; Streets, D.G.; He, K.; Tsay, S.-C.; Gleason, J.F. Recent large reduction in sulfur dioxide emissions from Chinese power plants observed by the Ozone Monitoring Instrument. *Geophys. Res. Lett.* **2010**, *37*. [CrossRef]
- Zhang, Q.; Geng, G.; Wang, S.; Richter, A.; He, K. Satellite remote sensing of changes in NO<sub>x</sub> emissions over China during 1996–2010. *Chin. Sci. Bull.* **2012**, *57*, 2857–2864. [CrossRef]
- Koukouli, M.E.; Balis, D.S.; van der A, R.J.; Theys, N.; Hedelt, P.; Richter, A.; Krotkov, N.; Li, C.; Taylor, M. Anthropogenic sulphur dioxide load over China as observed from different satellite sensors. *Atmos. Environ.* **2016**, *145*, 45–59. [CrossRef]
- Wang, T.; Wang, P.; Theys, N.; Tong, D.; Hendrick, F.; Zhang, Q.; Van Roozendaal, M. Spatial and temporal changes in SO<sub>2</sub> regimes over China in the recent decade and the driving mechanism. *Atmos. Chem. Phys.* **2018**, *18*, 18063–18078. [CrossRef]
- van der A, R.J.; Mijling, B.; Ding, J.; Koukouli, M.E.; Liu, F.; Li, Q.; Mao, H.; Theys, N. Cleaning up the air: Effectiveness of air quality policy for SO<sub>2</sub> and NO<sub>x</sub> emissions in China. *Atmos. Chem. Phys.* **2017**, *17*, 1775–1789. [CrossRef]
- Bauwens, M.; Compernelle, S.; Stavrakou, T.; Müller, J.F.; Van Gent, J.; Eskes, H.; Levelt, P.F.; van der A, R.; Veeffkind, J.P.; Vlietinck, J.; et al. Impact of coronavirus outbreak on NO<sub>2</sub> pollution assessed using TROPOMI and OMI observations. *Geophys. Res. Lett.* **2020**, *47*, e2020GL087978. [CrossRef]
- Fan, C.; Li, Y.; Guang, J.; Li, Z.; Elnashar, A.; Allam, M.; de Leeuw, G. The Impact of the Control Measures during the COVID-19 Outbreak on Air Pollution in China. *Remote Sens.* **2020**, *12*, 1613. [CrossRef]
- Huang, G.; Sun, K. Non-negligible impacts of clean air regulations on the reduction of tropospheric NO<sub>2</sub> over East China during the COVID-19 pandemic observed by OMI and TROPOMI. *Sci. Total Environ.* **2020**, *745*, 141023. [CrossRef] [PubMed]
- Sarfraz, M.; Mohsin, M.; Naseem, S.; Kumar, A. Modeling the relationship between carbon emissions and environmental sustainability during COVID-19: A new evidence from asymmetric ARDL cointegration approach. *Environ. Dev. Sustain.* **2021**, *23*, 16208–16226. [CrossRef]
- Schneider, P.; van der A, R.J. A global single-sensor analysis of 2002–2011 tropospheric nitrogen dioxide trends observed from space. *J. Geophys. Res. Atmos.* **2012**, *117*, D16309. [CrossRef]
- Geddes, J.A.; Martin, R.V. Global deposition of total reactive nitrogen oxides from 1996 to 2014 constrained with satellite observations of NO<sub>2</sub>; columns. *Atmos. Chem. Phys.* **2017**, *17*, 10071–10091. [CrossRef]
- van der A, R.J.; Peters, D.H.M.U.; Eskes, H.; Boersma, K.F.; Van Roozendaal, M.; De Smedt, I.; Kelder, H.M. Detection of the trend and seasonal variation in tropospheric NO<sub>2</sub> over China. *J. Geophys. Res.* **2006**, *111*, D12317. [CrossRef]
- Queisser, M.; Burton, M.; Theys, N.; Pardini, F.; Salerno, G.; Caltabiano, T.; Varnam, M.; Esse, B.; Kazahaya, R. TROPOMI enables high resolution SO<sub>2</sub> flux observations from Mt. Etna, Italy, and beyond. *Sci. Rep.* **2019**, *9*, 957. [CrossRef]
- Fioletov, V.E.; McLinden, C.A.; Krotkov, N.; Moran, M.D.; Yang, K. Estimation of SO<sub>2</sub> emissions using OMI retrievals. *Geophys. Res. Lett.* **2011**, *38*, L21811. [CrossRef]

22. Wang, S.W.; Zhang, Q.; Streets, D.G.; He, K.B.; Martin, R.V.; Lamsal, L.N.; Chen, D.; Lei, Y.; Lu, Z. Growth in NO<sub>x</sub> emissions from power plants in China: Bottom-up estimates and satellite observations. *Atmos. Chem. Phys.* **2012**, *12*, 4429–4447. [CrossRef]
23. Jin, J.; Ma, J.; Lin, W.; Zhao, H.; Shaiganfar, R.; Beirle, S.; Wagner, T. MAX-DOAS measurements and satellite validation of tropospheric NO<sub>2</sub> and SO<sub>2</sub> vertical column densities at a rural site of North China. *Atmos. Environ.* **2016**, *133*, 12–25. [CrossRef]
24. Theys, N.; De Smedt, I.; Van Gent, J.; Danckaert, T.; Wang, T.; Hendrick, F.; Stavrou, T.; Bauduin, S.; Clarisse, L.; Li, C.; et al. Sulfur dioxide vertical column DOAS retrievals from the Ozone Monitoring Instrument: Global observations and comparison to ground-based and satellite data. *J. Geophys. Res. Atmos.* **2015**, *120*, 2470–2491. [CrossRef]
25. Irie, H.; Takashima, H.; Kanaya, Y.; Boersma, K.F.; Gast, L.; Wittrock, F.; Brunner, D.; Zhou, Y.; Van Roozendaal, M. Eight-component retrievals from ground-based MAX-DOAS observations. *Atmos. Meas. Tech.* **2011**, *4*, 1027–1044. [CrossRef]
26. Tian, X.; Xie, P.; Xu, J.; Li, A.; Wang, Y.; Qin, M.; Hu, Z. Long-term observations of tropospheric NO<sub>2</sub>, SO<sub>2</sub> and HCHO by MAX-DOAS in Yangtze River Delta area, China. *J. Environ. Sci.* **2018**, *71*, 207–221. [CrossRef]
27. Chan, K.L.; Wang, Z.; Ding, A.; Heue, K.P.; Shen, Y.; Wang, J.; Zhang, F.; Shi, Y.; Hao, N.; Wenig, M. MAX-DOAS measurements of tropospheric NO<sub>2</sub> and HCHO in Nanjing and a comparison to ozone monitoring instrument observations. *Atmos. Chem. Phys.* **2019**, *19*, 10051–10071. [CrossRef]
28. Griffin, D.; Zhao, X.; McLinden, C.A.; Boersma, F.; Bourassa, A.; Dammers, E.; Degenstein, D.; Eskes, H.; Fehr, L.; Fioletov, V.; et al. High-Resolution Mapping of Nitrogen Dioxide With TROPOMI: First Results and Validation Over the Canadian Oil Sands. *Geophys. Res. Lett.* **2019**, *46*, 1049–1060. [CrossRef]
29. Verhoelst, T.; Compernelle, S.; Pinardi, G.; Lambert, J.C.; Eskes, H.J.; Eichmann, K.U.; Fjæraa, A.M.; Granville, J.; Niemeijer, S.; Cede, A.; et al. Ground-based validation of the Copernicus Sentinel-5P TROPOMI NO<sub>2</sub> measurements with the NDACC ZSL-DOAS, MAX-DOAS and Pandora global networks. *Atmos. Meas. Tech.* **2021**, *14*, 481–510. [CrossRef]
30. Wang, C.; Wang, T.; Wang, P.; Rakitin, V. Comparison and Validation of TROPOMI and OMI NO<sub>2</sub> Observations over China. *Atmosphere* **2020**, *11*, 636. [CrossRef]
31. Zhao, X.; Griffin, D.; Fioletov, V.; McLinden, C.; Cede, A.; Tiefengraber, M.; Müller, M.; Bogner, K.; Strong, K.; Boersma, F.; et al. Assessment of the quality of TROPOMI high-spatial-resolution NO<sub>2</sub> data products in the Greater Toronto Area. *Atmos. Meas. Tech.* **2020**, *13*, 2131–2159. [CrossRef]
32. Ialongo, I.; Virta, H.; Eskes, H.; Hovila, J.; Douros, J. Comparison of TROPOMI/Sentinel-5 Precursor NO<sub>2</sub> observations with ground-based measurements in Helsinki. *Atmos. Meas. Tech.* **2020**, *13*, 205–218. [CrossRef]
33. Judd, L.M.; Al-Saadi, J.A.; Szykman, J.J.; Valin, L.C.; Janz, S.J.; Kowalewski, M.G.; Eskes, H.J.; Veefkind, J.P.; Cede, A.; Mueller, M.; et al. Evaluating Sentinel-5P TROPOMI tropospheric NO<sub>2</sub> column densities with airborne and Pandora spectrometers near New York City and Long Island Sound. *Atmos. Meas. Tech.* **2020**, *13*, 6113–6140. [CrossRef]
34. Veefkind, J.P.; Aben, I.; McMullan, K.; Förster, H.; De Vries, J.; Otter, G.; Claas, J.; Eskes, H.J.; De Haan, J.F.; Kleipool, Q.; et al. TROPOMI on the ESA Sentinel-5 Precursor: A GMES mission for global observations of the atmospheric composition for climate, air quality and ozone layer applications. *Remote Sens. Environ.* **2012**, *120*, 70–83. [CrossRef]
35. Sentinel-5P Pre-Operations Data Hub. Available online: <https://s5phub.copernicus.eu/> (accessed on 14 September 2021).
36. Description of TROPOMI L2 Product—Nitrogen Dioxide. Available online: <http://www.tropomi.eu/data-products/nitrogen-dioxide> (accessed on 14 September 2021).
37. Description of TROPOMI L2 Product—Sulphur Dioxide. Available online: <http://www.tropomi.eu/data-products/sulphur-dioxide> (accessed on 14 September 2021).
38. Goddard Earth Sciences Data and Information Services Center. Available online: <https://disc.gsfc.nasa.gov/> (accessed on 14 September 2021).
39. OMNO2 Product Guidance Document. Available online: [https://aura.gesdisc.eosdis.nasa.gov/data/Aura\\_OMI\\_Level2/OMNO2.003/doc/README.OMNO2.pdf](https://aura.gesdisc.eosdis.nasa.gov/data/Aura_OMI_Level2/OMNO2.003/doc/README.OMNO2.pdf) (accessed on 15 September 2021).
40. Li, C.; Joiner, J.; Krotkov, N.A.; Bhartia, P.K. A fast and sensitive new satellite SO<sub>2</sub> retrieval algorithm based on principal component analysis: Application to the ozone monitoring instrument. *Geophys. Res. Lett.* **2013**, *40*, 6314–6318. [CrossRef]
41. Li, C.; Krotkov, N.A.; Leonard, P.J.T.; Carn, S.; Joiner, J.; Spurr, R.J.D.; Vasilkov, A. Version 2 Ozone Monitoring Instrument SO<sub>2</sub> product (OMSO2 V2): New anthropogenic SO<sub>2</sub> vertical column density dataset. *Atmos. Meas. Tech.* **2020**, *13*, 6175–6191. [CrossRef]
42. Wang, T.; Hendrick, F.; Wang, P.; Tang, G.; Clémer, K.; Yu, H.; Fayt, C.; Hermans, C.; Gielen, C.; Müller, J.F.; et al. Evaluation of tropospheric SO<sub>2</sub> retrieved from MAX-DOAS measurements in Xianghe, China. *Atmos. Chem. Phys.* **2014**, *14*, 11149–11164. [CrossRef]
43. Vandaele, A.C.; Hermans, C.; Simon, P.C.; Carleer, M.; Colin, R.; Fally, S.; Mérienne, M.; Jenouvrier, A.; Coquart, B. Measurements of the NO<sub>2</sub> absorption cross-section from 42,000 cm<sup>-1</sup> to 10,000 cm<sup>-1</sup> (238–1000 nm) at 220 K and 294 K. *J. Quant. Spectrosc. Radiat. Transf.* **1998**, *59*, 171–184. [CrossRef]
44. Vandaele, A.C.; Simon, P.C.; Guillemot, J.M.; Carleer, M.; Colin, R. SO<sub>2</sub> absorption cross section measurement in the UV using a Fourier transform spectrometer. *J. Geophys. Res. Atmos.* **1994**, *99*, D12. [CrossRef]
45. Bogumil, K.; Orphal, J.; Homann, T.; Voigt, S.; Spietz, P.; Fleischmann, O.C.; Vogel, A.; Hartmann, M.; Kromminga, H.; Bovensmann, H.; et al. Measurements of molecular absorption spectra with the SCIAMACHY pre-flight model: Instrument characterization and reference data for atmospheric remote-sensing in the 230–2380 nm region. *J. Photochem. Photobiol. A Chem.* **2003**, *157*, 167–184. [CrossRef]

46. Hermans, C.; Vandaele, A.C.; Fally, S.; Carleer, M.; Merienne, M.F. *Absorption Cross-Section of the Collision-Induced Bands of Oxygen from the UV to the NIR.*; Springer: Dordrecht, The Netherlands, 2003.
47. Rothman, L.S.; Barbe, A.; Benner, D.C.; Brown, L.R.; Camy-Peyret, C.; Carleer, M.R.; Chance, K.; Clerbaux, C.; Dana, V.; Devi, V.M.; et al. The HITRAN molecular spectroscopic database: Edition of 2000 including updates through 2001. *J. Quant. Spectrosc. Radiat. Transf.* **2003**, *82*, 5–44. [[CrossRef](#)]
48. Dimitropoulou, E.; Hendrick, F.; Pinardi, G.; Friedrich, M.M.; Merlaud, A.; Tack, F.; De Longueville, H.; Fayt, C.; Hermans, C.; Laffineur, Q.; et al. Validation of TROPOMI tropospheric NO<sub>2</sub> columns using dual-scan MAX-DOAS measurements in Uccle, Brussels. *Atmos. Meas. Tech.* **2020**, *13*, 5165–5191. [[CrossRef](#)]
49. Boersma, K.F.; Eskes, H.J.; Brinksma, E.J. Error analysis for tropospheric NO<sub>2</sub> retrieval from space. *J. Geophys. Res. Atmos.* **2004**, *109*, D04311. [[CrossRef](#)]
50. Xia, C.; Liu, C.; Cai, Z.; Duan, X.; Hu, Q.; Zhao, F.; Liu, H.; Ji, X.; Zhang, C.; Liu, Y. Improved Anthropogenic SO<sub>2</sub> Retrieval from High-Spatial-Resolution Satellite and its Application during the COVID-19 Pandemic. *Environ. Sci. Technol.* **2021**, *55*, 11538–11548. [[CrossRef](#)] [[PubMed](#)]
51. Filonchyk, M.; Hurynovich, V.; Yan, H.; Gusev, A.; Shpilevskaya, N. Impact Assessment of COVID-19 on Variations of SO<sub>2</sub>, NO<sub>2</sub>, CO and AOD over East China. *Aerosol. Air Qual. Res.* **2020**, *20*, 1530–1540. [[CrossRef](#)]
52. Wang, T.; Wang, P.; Hendrick, F.; Van Roozendael, M. Re-examine the APEC blue in Beijing 2014. *J. Atmos. Chem.* **2018**, *75*, 235–246. [[CrossRef](#)]